Supplementary Information

Ideal two-dimensional solid electrolytes for fast ions transport: metal trihalides MX_3 with intrinsic atomic pores

Maokun Wu,[a] Pan Liu,[a] Luyan Li,[b] Hong Dong,[a] Yahui Cheng,[a] Haijun Chen,[a]

Weichao Wang,[a] Hui Liu,[a] FengLu,[a,] Wei-Hua Wang,[a,*] Kyeongjae Cho [c,*]*

[a]Department of Electronic Science and Engineering, and Key Laboratory of Photo-Electronic Thin Film Device and Technology of Tianjin, Nankai University, Tianjin 300350, P. R. China

[b]School of Science, Shandong Jianzhu University, Jinan 250101, China

[c]Department of Materials Science and Engineering, The University of Texas at Dallas, Richardson, TX 75080, USA

Email addresses: whwangnk@nankai.edu.cn; lufeng@nankai.edu.cn; kjcho@utdallas.edu

S1. The optimized structural parameters of monolayer MX_3-ion systems

Table S1 The optimized structural parameters of monolayer MX_3-ion systems. The pore size of monolayer MX_3 (r in Å) and the vertical distance from the metal ion to the M atoms plane (d in Å). d=0.0 Å represents that the ion is located within the M atoms plane.

	$ScCl_3$		$ScBr_3$		AsI_3		ScI_3	
	r (Å)	d (Å)	r (Å)	d (Å)	r (Å)	d (Å)	r (Å)	d (Å)
Pristine MX_3	4.72	/	4.91	/	5.18	/	5.26	/
MX_3-Li^+	4.46	0.00	4.69	0.00	5.05	0.00	5.09	0.00
MX_3-Na^+	4.71	2.81	4.97	2.90	5.28	0.00	5.40	2.64
MX_3-K^+	4.72	3.59	4.93	3.77	5.30	3.96	5.32	3.98
MX_3-Mg^{2+}	4.28	0.00	4.52	0.00	4.89	0.00	4.95	0.00
MX_3-Ca^{2+}	4.66	2.82	4.96	2.78	5.22	0.00	5.26	0.00
	YBr_3		SbI_3		YI_3		BiI_3	
	r (Å)	d (Å)	r (Å)	d (Å)	r (Å)	d (Å)	r (Å)	d (Å)
Pristine MX_3	5.29	/	5.42	/	5.51	/	5.53	/
MX_3-Li^+	4.90	0.00	5.11	0.00	5.20	0.00	5.18	0.00
MX_3-Na^+	5.34	0.00	5.39	0.00	5.45	0.00	5.44	0.00
MX_3-K^+	5.31	3.61	5.61	3.80	5.55	3.87	5.70	3.76
MX_3-Mg^{2+}	4.61	0.00	4.87	0.00	4.96	0.00	4.90	0.00
MX_3-Ca^{2+}	5.03	0.00	5.24	0.00	5.30	0.00	5.25	0.00

S2. Diffusion time of ions travelling through monolayer MX_3

Table S2 Diffusion time τ(ion) (s) of metal ions through monolayer MX_3.

	$ScCl_3$	$ScBr_3$	AsI_3	ScI_3	YBr_3	SbI_3	YI_3	BiI_3
$\tau(Li^+)$	4.67×10^{-5}	1.98×10^{-3}	7.58×10^{-5}	3.69×10^{-4}	5.92×10^{-6}	5.05×10^{-6}	3.92×10^{-5}	8.06×10^{-6}
$\tau(Na^+)$	4.85×10^{-11}	7.96×10^{-9}	1.88×10^{-5}	4.42×10^{-7}	2.62×10^{-6}	8.20×10^{-5}	9.90×10^{-5}	1.46×10^{-4}
$\tau(K^+)$	1.28×10^{2}	1.16×10^{-4}	1.40×10^{-9}	3.73×10^{-8}	3.09×10^{-10}	9.52×10^{-10}	3.48×10^{-10}	3.40×10^{-9}
$\tau(Mg^{2+})$	5.62×10^{10}	1.02×10^{12}	2.67×10^{0}	1.04×10^{11}	1.17×10^{11}	9.62×10^{0}	2.14×10^{10}	1.67×10^{4}
$\tau(Ca^{2+})$	1.07×10^{-3}	5.59×10^{-2}	1.60×10^{4}	2.19×10^{9}	5.99×10^{7}	8.93×10^{5}	9.62×10^{10}	9.01×10^{8}

S3. Phonon spectra of MX_3-Li^+ complexes

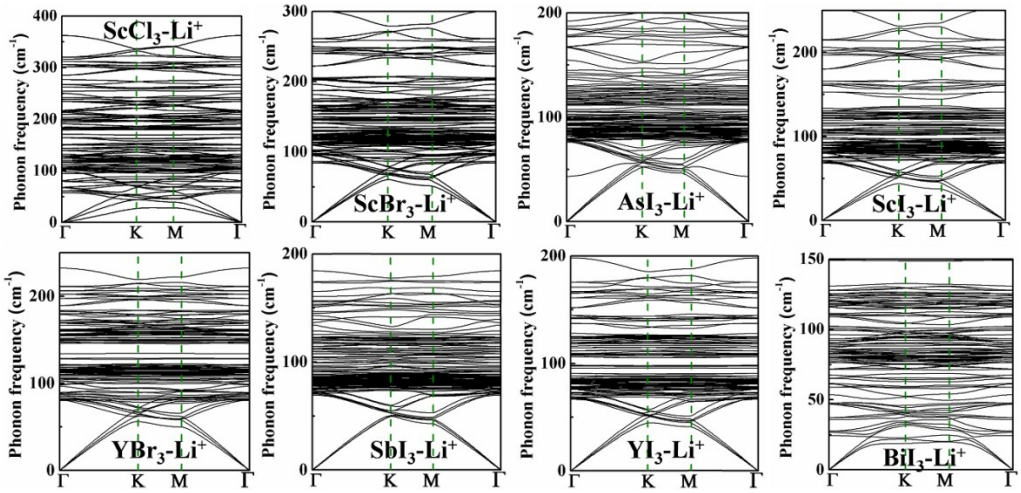

Fig. S1 (Color online) Phonon dispersions for MX_3-Li^+ systems along high symmetric directions.

S4. Band structures of pristine $ScCl_3$ and $ScCl_3$-Li^+ complex

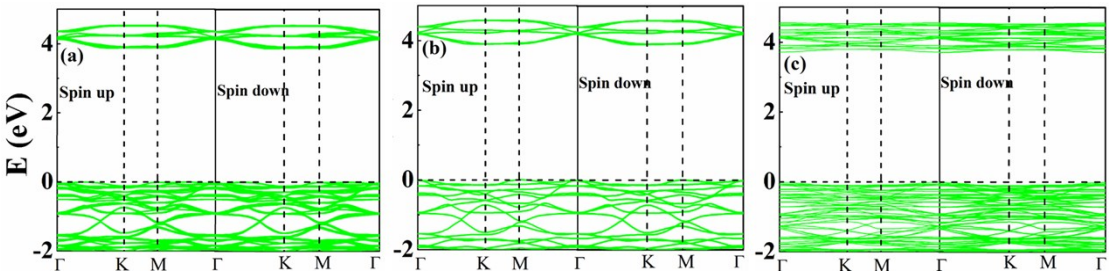

Fig. S2 (Color online) Band structures of spin-up and spin-down channels for (a) bulk $ScCl_3$, (b) monolayer $ScCl_3$, and (c) monolayer $ScCl_3$-Li^+ systems. The Fermi level marked by the horizontal dashed lines is set as a value of zero.

The non-magnetic state for all pristine MX_3 and MX_3-ion complexes has been converged through initial setting up spin-polarized state. The band structures of bulk $ScCl_3$, monolayer $ScCl_3$ and $ScCl_3$-Li^+ complex as examples are displayed in Fig. S2, where the spin up and spin down channels are symmetric. It is also consistent with the literature reports on bulk $ScCl_3$.[1] In addition, the non-magnetic states and insulating character of MX_3 are kept intact during the ions transport because empty or fully occupation of M-3*d* (4*d*) orbitals is almost unchanged.

S5. Electronic states of ions travelling through monolayer MX_3 with HSE06 functional

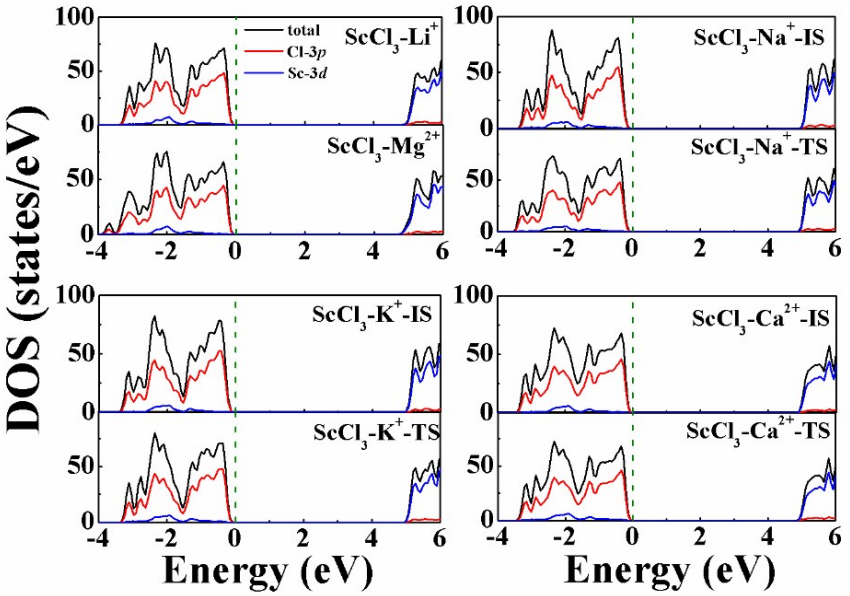

Fig. S3 (Color online) Density of states (DOS) and partial DOS (PDOS) of $ScCl_3$-ion complexes under the initial state (IS) and transition state (TS) with HSE06 method. (a) $ScCl_3$-Li^+/Mg^{2+}-TS, (b) $ScCl_3$-Na^+, (c) $ScCl_3$-K^+, (d) $ScCl_3$-Ca^{2+}. The Fermi level is set to be 0 eV.

S6. Band structures of MX_3-ion systems with PBE and PBE+SOC methods

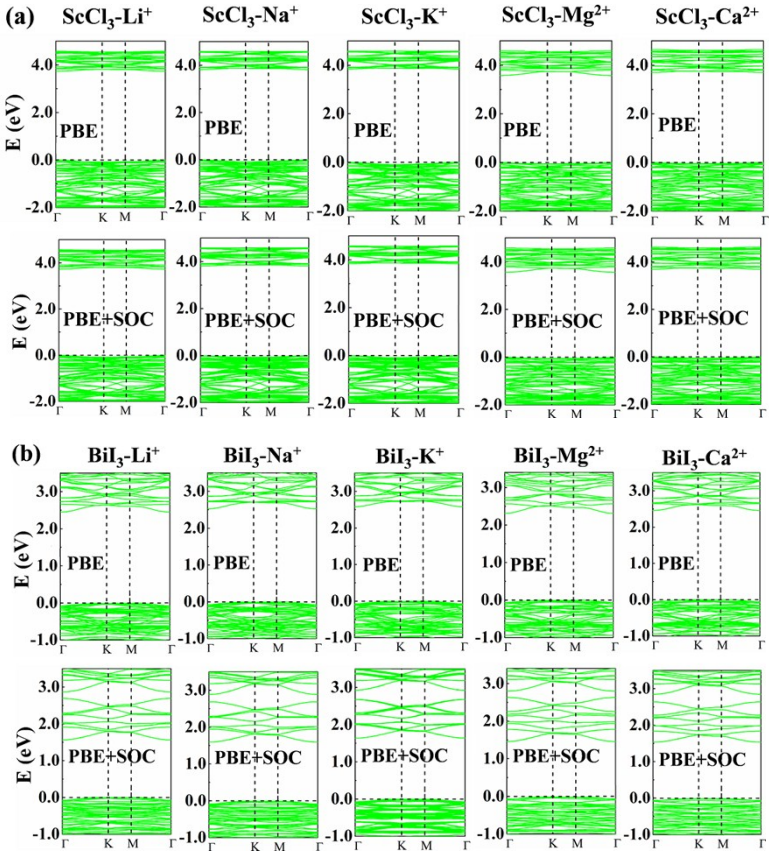

Fig. S4 (Color online) The band structures of (a) $ScCl_3$-ion and (b) BiI_3-ion systems with PBE and PBE+SOC methods. The Fermi level marked by the horizontal dashed lines is set as 0.

S7. The relative energy curves of ions diffusion in multilayered $ScCl_3$

About the ion diffusion in multilayered $ScCl_3$ in Fig. S5, the diffusion pathway is divided into the step 1 of intralayer diffusion and step 2 of interlayer diffusion. For step 1 transport, the ion in initial state is not trapped within the Sc atoms plane due to the interaction between adjacent layers. For Li^+ and Mg^{2+} with smaller ionic radius, E_a of Li^+ and Mg^{2+} transporting through multilayered $ScCl_3$ are reduced to ~0.12 eV and ~0.55 eV in step 1 relative to the monolayer transport. In contrast, Na^+ and Ca^{2+} show enhanced E_a of ~0.36 eV and 0.81 eV through multilayered $ScCl_3$. In addition, it is still difficult for K^+ to pass through $ScCl_3$ with E_a of ~0.91 eV. For step 2 transport, the energy barrier curves behave like volcanos, and the E_a increases with the ion mass.

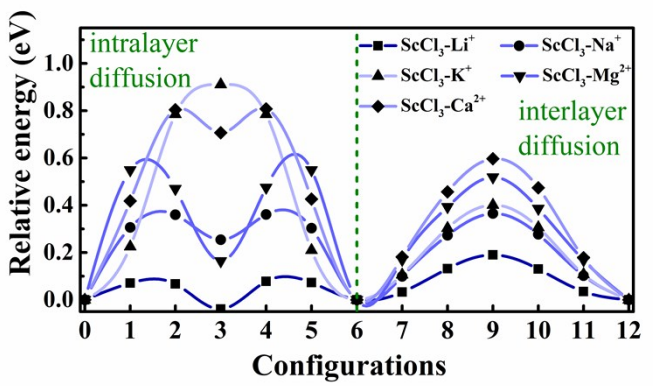

Fig. S5 (Color online) The relative energy curves of ions diffusion in multilayered $ScCl_3$. Left side and right side correspond to the step 1 of intralayer diffusion and the step 2 of interlayer diffusion.

S8. Diffusion time of ions transport through one layer of multilayered MX_3

Table S3 Diffusion time τ(ion) (in s) of metal ions travelling through one layer of multilayered MX_3.

	$ScCl_3$	$ScBr_3$	AsI_3	ScI_3	YBr_3	SbI_3	YI_3	BiI_3
$\tau(Li^+)$	1.61×10^{-10}	1.34×10^{-9}	2.27×10^{-8}	1.37×10^{-8}	2.98×10^{-11}	9.08×10^{-11}	5.09×10^{-10}	1.36×10^{-9}
$\tau(Na^+)$	2.44×10^{-7}	5.81×10^{-7}	8.06×10^{-6}	4.02×10^{-6}	3.07×10^{-8}	4.03×10^{-8}	1.10×10^{-7}	2.48×10^{-7}
$\tau(K^+)$	1.87×10^{2}	2.82×10^{-4}	3.36×10^{-5}	2.99×10^{-5}	9.38×10^{-7}	6.78×10^{-8}	8.20×10^{-7}	2.53×10^{-6}
$\tau(Mg^{2+})$	2.13×10^{-4}	2.82×10^{-4}	1.95×10^{-3}	1.02×10^{-2}	3.32×10^{-7}	2.11×10^{-6}	7.19×10^{-6}	2.94×10^{-6}
$\tau(Ca^{2+})$	3.65×10^{0}	4.27×10^{-2}	0.43×10^{0}	0.54×10^{0}	5.94×10^{-4}	9.76×10^{-5}	1.14×10^{-2}	3.57×10^{-3}

S9. Electronic structures of multilayered MX_3-ion complexes during ions diffusion process

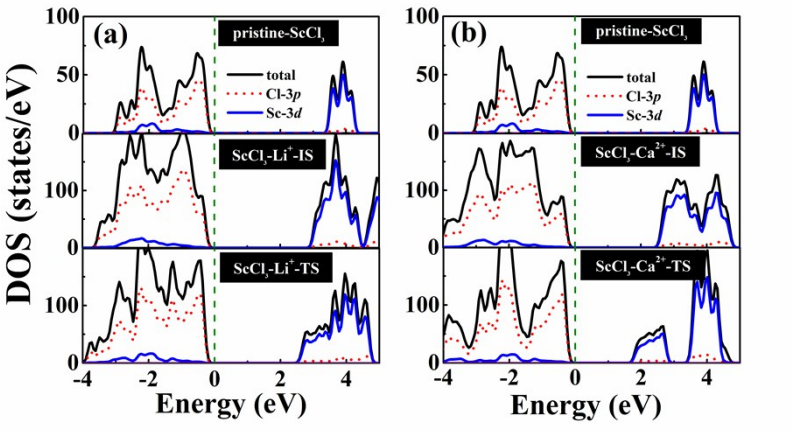

Fig. S6 (Color online) Density of states (DOS) of pristine $ScCl_3$ and Li^+/Ca^{2+} diffusion in bulk $ScCl_3$ in initial state (IS) and transition state (TS) with PBE functional. (a) $ScCl_3$-Li^+ (b) $ScCl_3$-Ca^{2+}. The Fermi level is set to be 0 eV.

The insulating character of multilayered MX_3 is well reserved during the ions diffusion process as shown in Fig. S6. In order to look into the influence of the ions diffusion on the band edges positions, the local density of states (LDOS) of multilayered $ScCl_3$-Li^+/Ca^{2+} systems at the initial state (IS) and final state (FS) during the intralayer diffusion step are displayed in Fig. S7. In fact, Li^+/Ca^{2+} is located within $ScCl_3$ layer-3rd and layer-1st in the IS considering the periodic boundary conditions. It is found that the band edges of $ScCl_3$ layer-3rd and layer-1st shift down and those of layer-2nd are retained, which is demonstrated in Fig. S7(b) and Fig. S7(c). In the TS, the Li^+/Ca^{2+} is within the pore in $ScCl_3$ layer-3rd. The band edges of the layer-3rd shift down and those of the other two layers are intact in Fig. S7(e) and Fig. S7(f). The band edges shift is due to the attraction interaction between the Li^+/Ca^{2+} and the electrons from the nearest $ScCl_3$ layer. Nevertheless, it is noted that no carriers transfer among $ScCl_3$ layers occurs and the insulating behavior is not affected by the ions travelling.

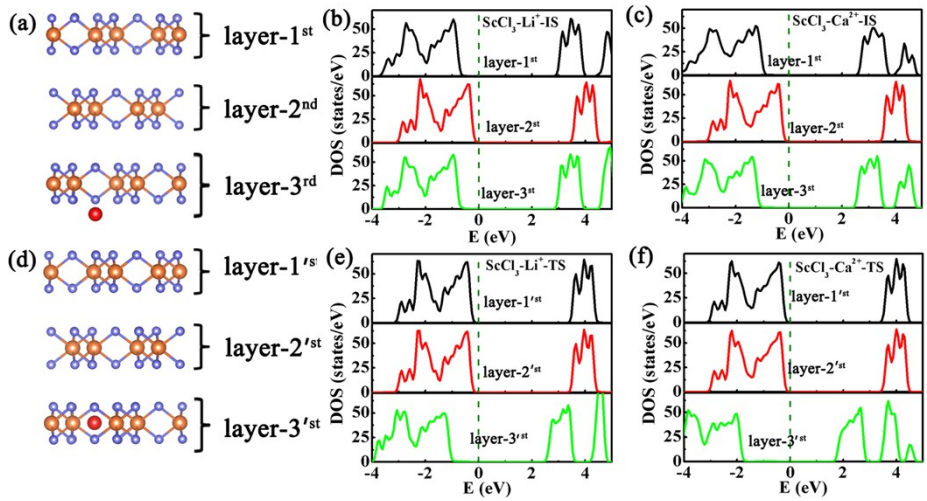

Fig. S7 (Color online) The schematic structure of IS in (a) and that of TS in (d) for intralayer diffusion of Li^+, Ca^{2+} through multilayered $ScCl_3$. The local density of states (LDOS) projected at different layers for $ScCl_3$-Li^+-IS in (b), $ScCl_3$-Ca^{2+}-IS in (c), $ScCl_3$-Li^+-TS in (e), and $ScCl_3$-Ca^{2+}-TS in (f). The Fermi level is set as 0 eV.

S10. Li^+ ions transport affected by ions density

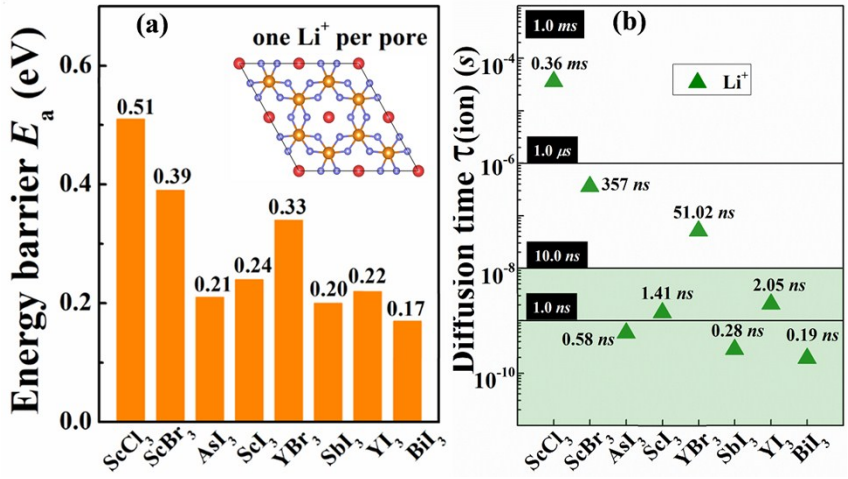

Fig. S8 (Color online) The energy barriers (E_a in eV) in (a) and diffusion time τ(ion) (s) in (b) of Li^+ transporting through one layer of MX_3 when the ions density increases. The inset shows the top view of schematic structures. The red balls represent Li^+ ions.

Since the ions transport through 2D MX_3 might be affected by the increased ions density, here the Li^+ transport performance through few layers MX_3 has been examined when the ions density increases, e.g. one Li^+ per atomic pore. As shown in Fig. S8, within one layer of $ScCl_3$ and $ScBr_3$ possessing small pore size, the diffusion energy barrier (E_a) of Li^+ actually increases with the increase of Li^+ density. The present increased E_a, 0.51 eV and 0.39 eV in

Fig. S8(a), corresponds to the diffusing time of 0.36 *ms* and 357 *ns*. In contrast, E_a is still small in the range of 0.17 eV-0.33 eV for Li^+ transporting through one layer of AsI_3, ScI_3, YBr_3, SbI_3, YI_3 and BiI_3 with large pore size. Consequently, the fast transport time through one layer of MX_3 (0.58 *ns*, 1.41 *ns*, 51.02 *ns*, 0.28 *ns*, 2.05 *ns* and 0.19 *ns*) is well preserved in these systems.

S11. Stability of Li_xMX_3 with the increase of Li^+ ions density

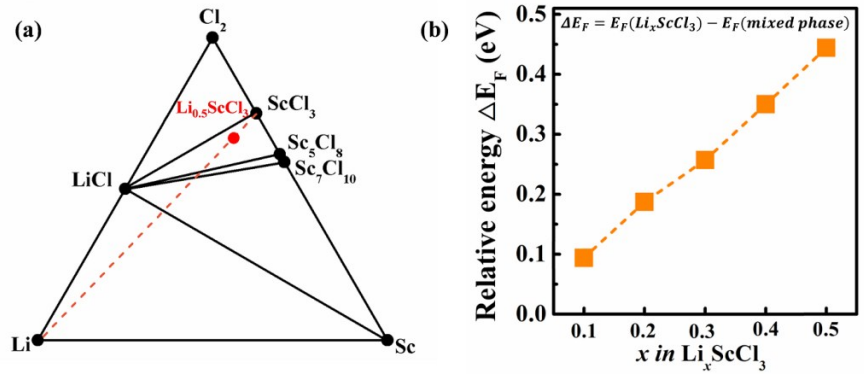

Fig. S9 (Color online) (a) Compositional phase diagram of Li-Sc-Cl. The black dots represent the stable phases. The red dot denotes $Li_{0.5}ScCl_3$. The dashed line indicates the $ScCl_3$-Li compositional space. (b) Formation energy difference between Li_xScCl_3 and the mixed phase with the increase of the ions density.

The chemical formula of 2D solid electrolytes in this work could be treated as Li_xMX_3 after the external Li^+ ions are introduced. In the following, the stability of Li_xMX_3 dependent on ions density is considered. Here Li-Sc-Cl is taken as an example and its phase stability is studied by constructing compositional phase diagram in Fig. S9(a).[1,2] At x=0, the pristine $ScCl_3$ is thermodynamically stable. The high ions density phase under one Li^+ per pore in one layer, corresponding to the chemical formula $Li_{0.5}ScCl_3$, is located within the triangle connected by LiCl, $ScCl_3$ and Sc_5Cl_8. It implies that $Li_{0.5}ScCl_3$ possibly decomposes into mixed phase including LiCl, $ScCl_3$ and Sc_5Cl_8. Nonetheless, the formation energy difference between Li_xScCl_3 and the mixed phase, $\Delta E_F = E_F(Li_xScCl_3) - E_F(mixed\ phase)$, is small in the range of ~0.10 eV-0.45 eV in Fig. S9(b). However, the decomposition reaction is not only determined by the thermodynamical stability, but also by the kinetics of chemical reactions. For $Li_{0.5}ScCl_3$, $ScCl_3$ is the host and the Li^+ ions are regarded as dopants. The prerequisite to decompose Li_xScCl_3 and generate LiCl is breaking the bond of Sc-Cl. Referring to bond

dissociation energy (BDE) data, it is as large as ~3.45 eV for Sc-Cl.[3] Besides, the large BDEs of Sc-Br (~4.62 eV), Y-Br (~5.01 eV), Y-I (~4.40 eV), and Bi-I (~1.94 eV) also demonstrate that it is hard to break M-X bond in these 2D MX_3 solid electrolytes.[3] Combined with above discussions, it is not easy to form LiX or NaX in Li_xMX_3 or Na_xMX_3 due to large kinetic barriers involving bond breaking for the necessary reactions. Similarly, the chemical stability of MX_3 contacting with Li metal electrode is characterized by decomposition reaction energy (ΔE_D) and kinetic reaction barrier. The ΔE_D of $ScCl_3$, $ScBr_3$, ScI_3, YBr_3 and YI_3 is in the range of -0.41 eV to -0.68 eV, which is much smaller than the currently used solid electrolytes, e.g., LGPS (-1.25 eV) and Li_3PS_4 (-1.42 eV).[4,5] Considering the large kinetic barriers in the necessary reactions to break bonds of M-X, $ScCl_3$, $ScBr_3$, ScI_3, YBr_3 and YI_3 as solid electrolytes contacting with Li metal would be stable.

References

1. A. Jain, G. Hautier, C. J. Moore, S. P. Ong, C. C. Fischer, T. Mueller, K. A. Persson and G. Ceder, *Comput. Mater. Sci.*, 2011, 50, 2295-2310.
2. S. P. Ong, L. Wang, B. Kang and G. Ceder, *Chem. Mater.* 2008**,** 20*,* 1798-1807.
3. Y. R. Luo, *Comprehensive Handbook of Chemical Bond Energies*, CRC Press, 2007.
4. Y. Zhu, X. He and Y. Mo, *ACS Appl. Mater. Interfaces*, 2015, 7, 23685-23693.
5. Y. Zhu, X. He and Y. Mo, *J. Mater. Chem. A*, 2016, 4, 3253-3266.